Structural Characterization of Type II Dockerin Module from the Cellulosome of *Clostridium thermocellum*: Calcium-Induced Effects on Conformation and Target Recognition†

Jarrett J. Adams,‡ Bradley A. Webb,‡ Holly L. Spencer,‡ and Steven P. Smith*,‡,§

Department of Biochemistry and Protein Function Discovery Group, Queen's University, Kingston, Ontario, Canada K7L 3N6

Received September 10, 2004; Revised Manuscript Received December 2, 2004

ABSTRACT: The assembly of a functional cellulose-degrading complex termed the cellulosome involves two specific calcium-dependent cohesin−dockerin interactions: type I and type II. Extensive structural and mutagenesis studies have been performed on the type I modules and their interaction in an attempt to identify the underlying molecular determinants responsible for this specificity. However, very little structural information exists for the type II interaction. We have performed a variety of biophysical studies on the type II dockerin−X-module modular pair (DocX), which comprises the C-terminal region of cellulosomal scaffoldin subunit from *Clostridium thermocellum*, to determine the effect of calcium on its structure and interaction with type II cohesin. Our results indicate that calcium binding to type II dockerin occurs with an apparent dissociation constant (K_d) of 7 μM, induces stable secondary and tertiary structure, and leads to the exposure of a hydrophobic surface. Calcium binding also results in the homodimerization of DocX. Analytical ultracentrifugation experiments indicate that the DocX homodimer has an elongated shape and a K_d of approximately 40 μM. However, addition of the SdbA type II cohesin binding partner led to the dissociation of the DocX homodimer and to the formation of a 1:1 heterodimer. We propose that the exposed hydrophobic surface forms, at least in part, the type II cohesin-binding site, which in the absence of cohesin results in the dimerization of DocX

Cellulosomes are large, surface-bound, extracellular multienzyme complexes responsible for the degradation of crystalline cellulose and associated plant cell wall polysaccharides. First identified in the thermophilic anaerobe *Clostridium thermocellum* (*1*, *2*), cellulosomes have now been characterized in a variety of other anaerobic bacteria, including *Clostridium celluloyticum* (*3*, *4*), *Clostridium cellulovorans* (*5*), *Clostridium josui* (*6*), *Acetivibrio cellulolyticus* (*7*, *8*), and *Bacteroides cellulosolvens* (*9*, *10*), as well as ruminal bacteria (*11*) and anaerobic fungi (*12*). The general quaternary architecture of cellulosomes includes numerous catalytic subunits constituting a variety of cellulases and hemicellulases, which are organized on a large, multimodular, noncatalytic scaffoldin subunit to form a single macromolecular machine able to efficiently and synergistically breakdown crystalline cellulose (*13*, *14*). A highly conserved noncatalytic module, termed dockerin, of the catalytic subunits is responsible for anchoring each enzyme to the scaffoldin subunit (*15*−*17*).

The *C. thermocellum* scaffoldin subunit, CipA, comprises a carbohydrate-binding domain (CBD),[1] nine highly conserved cohesin modules (C), a hydrophilic X module of unknown function (X), and a C-terminal dockerin module (D), which is divergent in sequence from the catalytic dockerin modules (Figure 1) (*18*, *19*). The cohesin modules form noncovalent interactions with the dockerin modules of the catalytic subunits, designated type I, though there appears to be very little discrimination between the various enzyme-associated dockerin modules (*20*−*24*). Contrary to this promiscuity, the specific interaction between the CipA C-terminal dockerin module and the cohesin modules of cell surface subunits, designated type II, tethers the cellulosome to the bacterial cell surface (*21*, *25*, *26*). Despite their specificity, both types of cohesin−dockerin interactions have a strong requirement for calcium that can be sequentially

† J.J.A. is a recipient of a McLaughlin Graduate Scholarship. B.A.W. is a recipient of an Ontario Graduate Scholarship. This research was supported by Canadian Institutes of Health Research Operating Grant MOP-53193 (S.P.S.). Infrastructure used in this study was funded through Canadian Foundation for Innovation and Ontario Innovation Trust.

* To whom correspondence should be addressed: Tel (613) 533-3188; fax (613) 533-2497; e-mail sps1@post.queensu.ca.

‡ Department of Biochemistry.

§ Protein Function Discovery Group.

[1] Abbreviations: ANS, 8-anilino-1-naphthalenesulfonate; AUC, analytical ultracentrifugation; CBD, cellulose-binding domain; CipA, *Clostridium thermocellum* scaffoldin subunit; CD, circular dichroism; Doc, *Clostridium thermocellum* scaffoldin subunit type II dockerin module; DocX (apo-, Ca-), *Clostridium thermocellum* scaffoldin subunit dockerin−X modular pair (calcium-free, calcium-bound); DSS, 2,2-dimethyl-2-silapentane-5-sulfonate; DTT, dithiothreitol; EDTA, ethylenediaminetetraacetic acid; GST, glutathione-S-tranferase; HEPES, 4-(2-hydroxyethyl)-1-piperazineethanesulfonic acid; HSQC, heteronuclear single quantum correlation; IPTG, isopropyl β-D-thiogalactopyranoside; K_d, dissocation constant; MALS, multiangle light scattering; MBP, maltose-binding protein; NMR, nuclear magnetic resonance; ppm, parts per million; SDS−PAGE, sodium dodecyl sulfate−polyacrylamide gel electrophoresis.

10.1021/bi048039u CCC: $30.25
Published on Web 01/22/2005

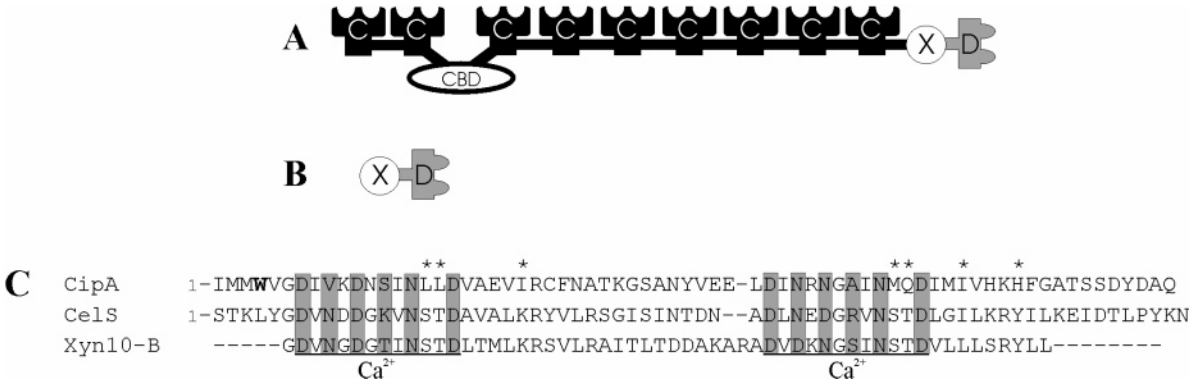

FIGURE 1: Schematic representations of (A) the CipA scaffoldin subunit of *Clostridium thermocellum*, where C = type I cohesin, CBD = carbohydrate-binding domain; X = X-module of unknown function, and D = type II dockerin module; and (B) X-module−Doc modular pair construct. (C) Protein sequence of type II dockerin. Underlined regions depict the two EF-hand calcium-binding motifs, and the shaded regions define the residues involved in calcium coordination. The single tryptophan residue used in intrinsic fluorescence studies of CipA DocX is shown in boldface type; asterisks identify residues located on the cohesin-binding surface of type I dockerin whose physical properties are significantly different in the type II dockerin.

ascribed to the two EF-hand calcium-binding motifs of the dockerin modules (*22*, *26*, *27*).

Identification of the molecular determinants dictating cohesin binding and specificity for the cohesin−dockerin interaction has been aided by recent structural and mutagenesis studies, which have primarily focused the on the type I interaction. Type I dockerin undergoes a calcium-induced folding event that stabilizes a tertiary structure (*28*), and recent structures of CelS type I dockerin (*29*) and the Xyn-10B type I dockerin−CipA type I cohesin complex (*30*) indicate that the dockerin structure becomes more compact upon binding to type I cohesin. Both calcium-binding segments of type I dockerin are required for cohesin recognition, and mutation of the conserved hydroxyl-containing residues at positions 10 and 11 of each calcium-binding motif in type I dockerin identified a role for them in type I cohesin binding and species specificity (*27*, *31*−*34*). The type I complex structure showed the hydroxyl groups of the serine and threonine residues in the second calcium-binding loop formed interface hydrogen bonds with the cohesin module (*30*). In contrast, very few studies on the type II interaction have been reported. Binding and dockerin mutagenesis studies have revealed a dissociation constant (K_d) of 1.8×10^{-9} M as well as the importance of positions 10 and 11 in the second calcium-binding loop for recognition of type II cohesin (*34*, *35*). However, a structural characterization of the type II dockerin module has not been reported.

In this study, we have generated a modular pair construct, comprising the C-terminal type II dockerin and the adjacent X-module from CipA of the *C. thermocellum* cellulosome (DocX), which is soluble at concentrations (millimolar) necessary for detailed biophysical and structural analyses. Using a combination of biochemical and biophysical techniques, we have demonstrated that upon calcium-induced folding of the dockerin module, recombinant DocX forms a noncovalent dimer, which dissociates to form a 1:1 complex with its biological ligand, SdbA type II cohesin module. Implications of these observations are made in relation to the type I dockerin, the architecture of CipA, and the specificity of the type I and type II dockerin−cohesin interactions.

MATERIALS AND METHODS

Subcloning of the DocX Modular Pair of the CipA Scaffoldin Subunit. The upstream and downstream primers GGAATTCCATATGAATAAACCTGTAATAGAAG and CCGCTCGAGCTGTGCGTCGTAATCAC, respectively, were used in a polymerase chain reaction (PCR) amplification with pCip102 (*36*) to generate a 510 bp fragment encoding the C-terminal region of CipA comprising the DocX modular pair, which also contained *Nde*I and *Xho*I sites (underlined). The *Nde*I−*Xho*I digested fragment was inserted into the *Nde*I and *Xho*I sites of the cloning region of a pET-21b expression vector (Stratagene) by use of T4 DNA ligase (Invitrogen). The sequence of the insert was confirmed by DNA sequencing and the plasmid was transformed into the *Escherichia coli* BL21 (DE3) strain for expression. The SdbA type II cohesin expression plasmid pCT1836, described in Smith et al. (*37*), was used .

Protein Expression and Purification. Expression of DocX involved the growth of transformed cells in 1 L of Luria−Bertani (LB) medium supplemented with 100 μg/L ampicillin in a 2.8 L Fernbach flask at 37 °C with shaking to an OD_{600} of 0.6. IPTG was added to a final concentration of 1 mM and growth was continued for an additional 4 h. The cells were harvested by centrifugation, resuspended in a volume of buffer A (25 mM Tris-HCl, pH 7.4, 250 mM NaCl, and 8 M urea) equal to 10 times their packed weight, and disrupted by sonication (3×30 s) at room temperature. Cell debris was removed by centrifugation for 1 h at 40 000 rpm in a Beckman Ti70 ultracentrifuge rotor. The supernatant solution was collected and applied to a column packed with 2 mL of Ni^{2+}-chelating Sepharose beads (Amersham Pharmacia Biotech) equilibrated with buffer A. The column was washed with 20 mL of buffer A containing 20 mM imidazole, and bound protein was eluted with buffer A containing 300 mM imidazole in 1 mL fractions. Fractions containing protein were determined by SDS−PAGE and subsequently pooled and dialyzed in buffer B (25 mM Tris-HCl, pH 7.4, 50 mM NaCl, and 10 mM EDTA). The refolded protein sample was applied to a Hi-Load 16/60 Superdex 75 size-exclusion column (Amersham Pharmacia Biosciences) equilibrated with buffer B and was eluted in 2 mL fractions with the same buffer. Fractions containing protein were pooled and concentrated on a Millipore Amicon 10 kDa centrifugal device

to a final volume of 5 mL and stored at −20 °C. Uniformly ^{15}N-labeled DocX was expressed and purified in a manner similar to that of the unlabeled protein, with the exception that 10 mL of LB overnight subculture was used to inoculate 1 L of M9 minimal medium containing 1 g/L $^{15}NH_4Cl$ and 10 mL of ^{15}N-Bio-Express-1000 medium (Cambridge Isotope Laboratories), and growth was continued for 14 h after IPTG induction. SdbA type II cohesin purification was performed in a manner similar to that reported previously (*37*), with the exception that a final size-exclusion step was performed, similar to that described above for DocX.

Circular Dichroism. Circular dichroism (CD) spectra were acquired on a rapid-scanning monochromator fitted with a CD module (RSM 1000, Olis Inc., Bogart GA). All far-UV spectra were recorded with a cuvette of 0.1 mm path length on samples containing 40 μM DocX in 2.5 mM HEPES, 1 mM β-mercaptoethanol, pH 7.0, and either 5 mM EDTA or 5 mM $CaCl_2$. Spectra were recorded from 260 to 185 nm and signal-averaged from nine scans recorded at 20 °C. The baseline was corrected by subtracting the spectra of the respective buffers collected under identical conditions. Percentage of secondary structure was calculated by use of the web-based program CDNN (*38*). Near-UV spectra were recorded in a 1.0 cm path length cylindrical quartz cuvette with a volume of 3 mL on samples of 150 μM Doc-X in 2.5 mM HEPES, 1 mM β-mercaptoethanol, pH 7.0, and either 5 mM EDTA or 5 mM $CaCl_2$. These spectra were averaged over eight scans. No smoothing was performed so that the fine structure of the spectra would be maintained. Molar ellipticity [θ] was calculated according to the formula $[\theta] = \theta \times 100/(nlc)$, where θ represents ellipticity, n represents the number of amino acids in the protein, l represents the path length in centimeters, and c represents the millimolar concentration.

Fluorescence Spectroscopy. All spectra were measured on a Perkin-Elmer LS50B luminescence spectrometer with 37 μM DocX in 25 mM HEPES, 25 mM NaCl, and 5 mM DTT, pH 7.0, at room temperature in a 1.5 mL 10 mm cuvette. The tryptophan fluorescence emission spectra and intensity changes were measured in the presence of 370 μM EDTA or 370 μM $CaCl_2$ with excitation and emission wavelengths of 295 nm and 300−450 nm, respectively, and slit widths of 4 nm. The calcium titration of DocX used exctitation and emission wavelengths of 295 and 350 nm, respectively, and a slit width of 15 nm. Incremental additions of calcium were added to 1.5 mL of 5 μM DocX and the emission intensities were averaged over 100 s/titration point, normalized to the zero titration point, and plotted against ligand concentration. The calcium binding curve was subjected to nonlinear regression analysis by use of the following hyperbolic equation: $y = (B_{max})(X)/K_d + X$, where B_{max} represents maximal fluorescence change, K_d is the calcium concentration at which DocX exhibits half-maximal binding, and X is the calcium concentration.

8-Anilino-1-naphthalenesulfonate (ANS) fluorescence spectroscopic studies were performed with 370 μM ANS in the presence of 5 mM EDTA or 5 mM $CaCl_2$ and recorded with excitation and emission wavelengths of 380 and 400−600 nm, respectively, and slit widths of 15 nm.

NMR Spectroscopy. ^{1}H−^{15}N HSQC NMR spectra of 0.5 mM uniformly ^{15}N-labeled DocX were recorded on a Varian INOVA 600 MHz spectrometer equipped with a pulse field gradient triple-resonance probe at 25 °C. The experiments used the enhanced sensitivity pulsed-field gradient approach by Kay et al. (*39*) and comprised a 1024 × 128 real data matrix, which was zero-filled once in each dimension. The proton chemical shifts were referenced to 0.0 ppm by use of the trimethylsilyl resonance of the DSS signal in the one-dimensional spectrum. The buffer conditions were 10 mM HEPES, 50 mM NaCl, 5 mM DTT (pH 7.0), 90% H_2O/10% D_2O, and either 5 mM EDTA or 5 mM $CaCl_2$. Spectra were processed and analyzed by use of NMRPipe (*40*) and NMRview (*41*), respectively.

Molar Mass Determination by Multiangle Light Scattering. Purified protein constructs at concentrations of 400 μM were eluted from a 50 mL S-200 Sephacryl size-exclusion column in 25 mM HEPES, pH 7.0, 25 mM NaCl, 5 mM DTT, 0.1% Tween 20, and either 10 mM EDTA or 10 mM $CaCl_2$ and passed directly through an absorbance monitor (LC-75 Perkin-Elmer) set at 280 nm and a DAWN-DSP multiangle light scattering detector (Wyatt Technology, Santa Barbara, CA), which were linked in tandem. Measurements of the mass concentration (grams per milliliter) from the absorbance monitor and the laser light scattered at 15°, 26°, 35°, 43°, 52°, 60°, 69°, 80°, 90°, 100°, 111°, 121°, 132°, 142°, 152°, and 163° angles were collected every 8.0 s by use of the Astra program (Wyatt Technology). The weight-averaged molecular weight (M_w) of the eluted proteins were calculated at any given point by regression analysis of the Debye plot (*42*), which involves a plot of $(K^*c)/R_\theta$ versus $\sin^2(\theta/2)$, where K^* is an optical constant, c is the weight concentration of the sample in grams per milliliter, R_θ is the Rayleigh ratio at a given angle [the ratio of the intensity of the light scattered by the solution (in excess over the solvent alone) to the intensity of the incident laser light], and θ is the angle of scattering. The molar mass is found from the regression of the Debye plot where $M_w = R_\theta/(K^*c)$ at $\theta = 0$ [i.e., $\sin^2(\theta/2) = 0$]. The M_w was calculated by the Astra 4.5 software by use of the following parameters: $\epsilon_{280nm} = 0.847$; refractive index gradient for protein $(\delta n/\delta c) = 0.192$ mL/g; refractive index for solvent = 1.3333; A_2 (second virial coefficient) = 0. The DAWN-DSP instrument was fitted with a K5 flow cell and a He−Ne laser (632.8 nm) and was calibrated with 0.02-nm-filtered toluene, and the detectors were normalized for the experiments on the monomer peak of bovine serum albumin (~98% monomeric bovine serum albumin; Sigma) gel-filtered on Sephacryl S-1000 in degassed, 0.2-μm-filtered 20 mM HEPES, 500 mM NaCl, and 0.001% Tween 80 as per manufacturer's instructions. The differences in the refractive indexes of the different buffer systems used were assumed to be negligible.

Size-Exclusion Chromatography. Analytical size-exclusion chromatography of purified constructs was carried out at 20 °C on a Superdex 75 (16/60) column connected to an ÄKTA fast protein liquid chromatographic (FPLC) system (Amersham Pharmacia Biosciences). The running buffer was composed of 25 mM HEPES, 25 mM NaCl, 5 mM DTT, pH 7.0, and either 5 mM EDTA or 5 mM $CaCl_2$. Protein constructs at concentrations of 531 μM were eluted at a flow rate of 1 mL/min with 2 mL fractions being collected and the optical density of the eluent being monitored at 280 nm. Molecular masses (M) were determined from a plot of log M vs V_e/V_0 (V_e = elution volume and V_0 = void volume). The standard curve was generated from the following protein

standards (*M*): bovine serum albumin (68 kDa), ovalbumin (45 kDa), and myoglobin (17 kDa).

Analytical Ultracentrifugation. Samples used in analytical ultracentrifugation (AUC) were dialyzed extensively against 25 mM HEPES, 25 mM NaCl, 5 mM DTT (pH 7.0), and either 10 mM EDTA or 10 mM $CaCl_2$, and dialysis buffer was saved and used in the reference sector for all runs. Prior to sedimentation analysis, samples were supplemented with 10 mM DTT to ensure full reduction of the single cysteine present in DocX. All AUC experiments were preformed at 20 °C. Sedimentation equilibrium analysis was preformed with a Beckman XL-I analytical ultracentrifuge with a four-hole An-60Ti rotor with 6-sector Epon charcoal center pieces. Data were collected at 280 nm at three rotor speeds (15 000, 18 000, and 21 000 rpm) and at three protein concentrations (0.2, 0.4, and 0.6 mg/mL). Absorbance measurements were taken at 0.002 cm radial steps and averaged over 10 observations. Data sets were collected after equilibrium was obtained, as judged by the successive overlay of scans at 2 h intervals. The partial specific volume and solution density were calculated by SEDNTERP (version 1.05, John Philo, 2000). The molecular weight for both a single ideal species and a monomer−dimer interaction were obtained from XL-A/XL-I data analysis software (version 6.03, Bechman/Microcal).

The sedimentation velocity analyses were carried out at 20 °C in cells containing double-sector Epon charcoal centerpieces. Velocity runs for DocX were conducted at 50 000 rpm by use of Rayleigh interference optics. Interference scans were taken at intervals of 1 min for 400 scans. Best-fit profiles according to the continuous distribution *c*(*S*) Lamm equation model from SEDFIT (*43*) were overlaid on the experimental data by use of every second scan.

RESULTS

Expression and Purification of Type II Dockerin-Containing Constructs. A clone expressing the isolated CipA type II dockerin module produced the 9 kDa N-terminal $(His)_6$-tagged polypeptide in the insoluble form. All attempts to renature the protein were unsuccessful (data not shown). Therefore, we constructed a clone encoding a C-terminal $(His)_6$-tagged modular pair comprising Doc and the adjacent hydrophilic X-module from CipA (Figure 1B), hereafter termed DocX, in an effort to counterbalance the insolubility of isolated Doc. Expression and purification of DocX were monitored by SDS−PAGE (Figure 2). Solubilized cell extract contained an intense band migrating at the approximate size of the DocX construct (M_r 18 816.1 Da; Figure 2, lane 2). Cell fractionation experiments showed that, similar to isolated Doc, DocX was localized primarily to the inclusion body fraction of *E. coli*. Denaturation of the whole cell lysate in 8 M urea was followed by a Ni^{2+} affinity chromatography purification step and refolding via dialysis in the absence of calcium (Figure 2, lane 3). Unlike Doc, apo-DocX remained soluble under native conditions, and a final size-exclusion chromatography step was performed that purified the protein to homogeneity (Figure 2, lane 4). Electrospray mass spectrometry verified the size and purity apo-DocX (observed molecular mass of 18 815.1 Da; theoretical molecular mass of 18 816.2 Da).

Circular Dichroism Spectroscopy. To assess the secondary and tertiary structure of DocX in the absence and presence

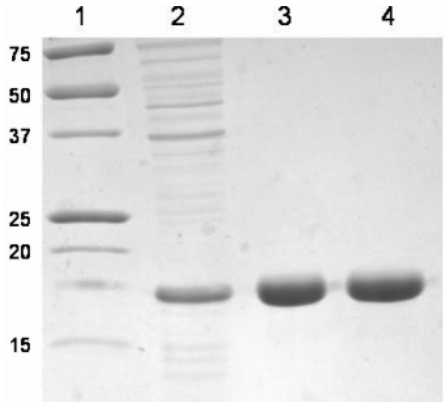

FIGURE 2: Expression and purification of recombinant fragments from the CipA scaffoldin subunit of *C. thermocellum* monitored by SDS−PAGE. Lane 1, molecular weight markers; lane 2, cell lysate from DocX induction (37 °C, 3 h); lane 3, supernatant after Ni^{2+}-affinity chromatography and dialysis into native conditions; lane 4, size-exclusion chromatography fraction.

of calcium, far- and near-UV CD spectroscopy were carried out at room temperature. A broad negative band in the far-UV CD spectrum of apo-DocX extended from 225 to 200 nm, indicating that in the absence of calcium this protein construct comprised primarily β and random coil structure (Figure 3A). Furthermore, the lack of a large positive band around 190 nm also suggested that apo-DocX contained regions of high flexibility or random coil structure. Deconvolution of the data by use of CDNN software (*38*) predicted 33% β-sheet, 23% β-turn, and 8% α-helix, which is quite similar to the elements of secondary structure predicted from CD and NMR studies of the isolated X-module (*44*). Addition of calcium to saturating levels led to a dramatic change in the far-UV CD spectrum of DocX (Figure 3A). A significant decrease in ellipticity between 230 and 203 nm, a crossover at 200 nm, and the appearance of a large positive band below 200 nm with a maximum of 191 nm all suggested that there was an increase in helical content. Deconvolution of the data suggested an approximate 2-fold increase in helical content (from 8% to 19%), a corresponding decrease in random coil and β-turn character, and a similar content of β-structure and turns to that of apo-DocX.

The sensitivity of the near-UV CD signal to the environment of aromatic amino side chains provides an excellent probe to monitor changes in tertiary structure of proteins. DocX has a total of six phenylalanine residues, one tryptophan residue, and eight tyrosine residues, and near-UV CD spectroscopy was used to assess the effects of calcium binding on the tertiary structure of DocX (Figure 3B). In the absence of calcium, a broad positive band extending from 244 to 268 nm and a negative band in the region between 270 and 295 nm was observed, illustrating the presence of defined tertiary structure involving phenylalanine and tyrosine residues. Upon addition of calcium, a pronounced broad positive band extended from 243 to 283 nm and the signal intensity was markedly greater than that of apo-DocX, indicative of a change in the tertiary structure for DocX in the calcium-bound state. Furthermore, the observation of a slight positive band centered at 295 nm and extending to 300 nm, not seen for apo-DocX, alluded to an altered environment of the single tryptophan residue (Figure 1C). Overall, the changes observed in the CD spectrum can be attributed to a calcium-induced change in the structure of

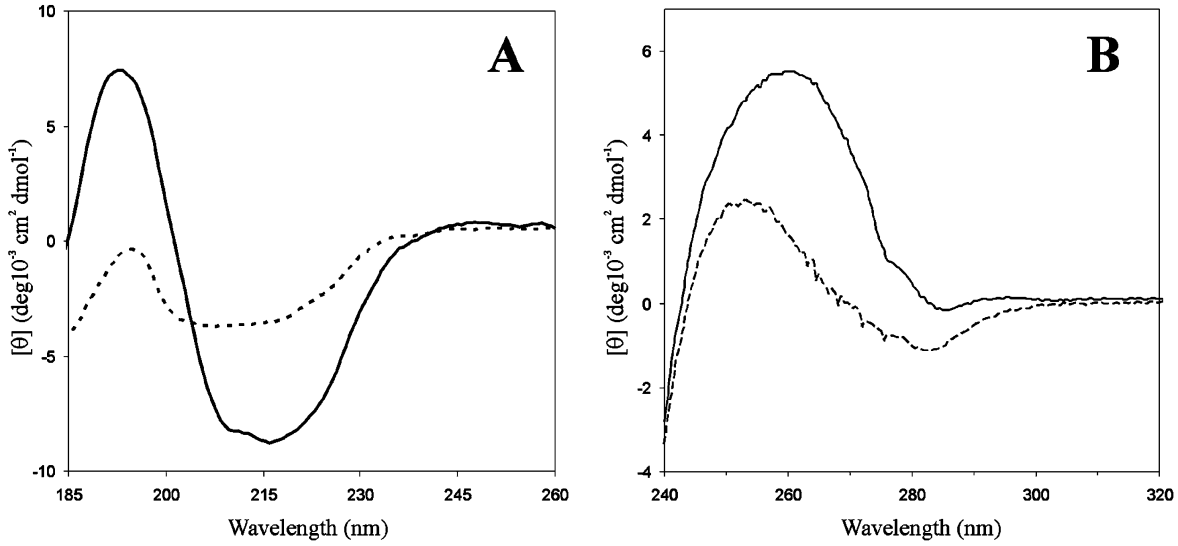

FIGURE 3: Calcium-induced conformational effects on DocX monitored by circular dichroism and intrinsic tryptophan fluorescence spectroscopy at pH 7.0 and room temperature. (A) Far-UV CD spectra of 40 μM apo-DocX (- - -) and 40 μM Ca-DocX (—). (B) Near-UV CD spectra of 150 μM apo-DocX (- - -) and 150 μM Ca-DocX (—).

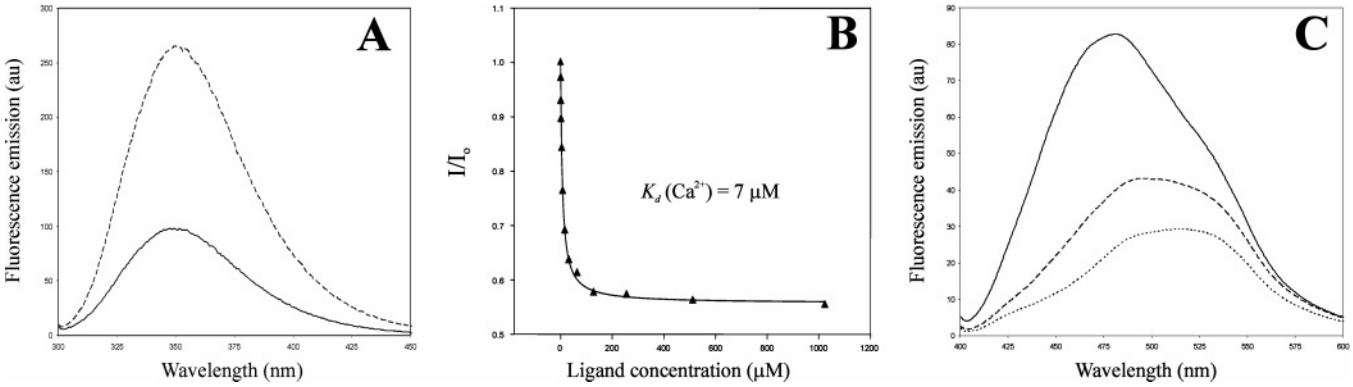

FIGURE 4: Calcium-induced conformational changes of DocX monitored by fluorescence spectroscopy. (A) Intrinsic tryptophan fluorescence emission spectra of 37 μM DocX in the absence (---) and presence (—) of calcium. (B) DocX dose-dependent binding to calcium (▲). (C) ANS fluorescence emission spectra used to monitor the exposed hydrophobic surface of apo-DocX (---), Ca-DocX (—), and ANS in the absence of DocX (•••). The *y*-axis represents fluorescence emission intensity in arbitrary units

the dockerin module of the DocX modular pair, given that calcium does not alter the CD spectrum of the isolated X-module (data not shown), that the dockerin module comprises two EF-hand calcium-binding motifs (Figure 1D), and that the sole tryptophan is located within the N-terminal sequence of the dockerin module (Figure 1D).

Intrinsic Tryptophan and ANS Fluorescence Spectroscopy. To further probe the effect of calcium on the conformation of DocX, and in particular on the lone tryptophan residue (Figure 1C), intrinsic tryptophan fluorescence spectroscopy was employed. As shown in Figure 4A, upon excitation at 295 nm, both apo- and Ca-DocX displayed broad emission spectra with a maximum of 350 nm, indicative of the tryptophan side chain occupying a solvent-accessible environment. However, a calcium-induced quenching of the tryptophan fluorescence was observed, with the emission intensity of DocX decreasing by 63% in the presence of calcium. This suggested either that a minor localized structural perturbation occurred in the region occupied by the tryptophan side chain or that the protein undergoes a major conformation transition. Furthermore, a calcium titration monitored by intrinsic tryptophan fluorescence determined the dissociation constant (K_d) of DocX−calcium interaction to be 7 μM (Figure 4B).

Several EF-hand calcium-binding proteins, including calmodulin (*45*), troponin C (*46*), and the S100 protein family (*47*, *48*), have been shown to undergo calcium-induced conformational changes that expose hydrophobic surfaces which are involved in target protein recognition. To probe these types of structural alterations, ANS, a hydrophobic compound, is commonly used due to characteristic changes in its fluorescence emission profile, including a blue shift and intensity increase. ANS fluorescence was therefore used to determine whether DocX undergoes a calcium-induced exposure of a hydrophobic region. As shown in Figure 4C, a blue shift (from 516 to 495 nm) in ANS fluorescence occurred in the presence of apo-DocX with a relatively modest 1.5-fold increase in intensity, while Ca-DocX caused a blue shift from 516 to 482 nm and a 2.8-fold increase in intensity, when compared to the emission spectrum of ANS alone. These results suggest that a region comprising hydrophobic residues is exposed in apo-DocX and that either this region becomes more exposed in the presence of calcium or additional hydrophobic regions become accessible upon calcium binding.

NMR Spectroscopy. To obtain greater insight into the extent of calcium-induced structural changes in DocX, we used 2D ^{1}H−^{15}N heteronuclear NMR spectroscopy to moni-

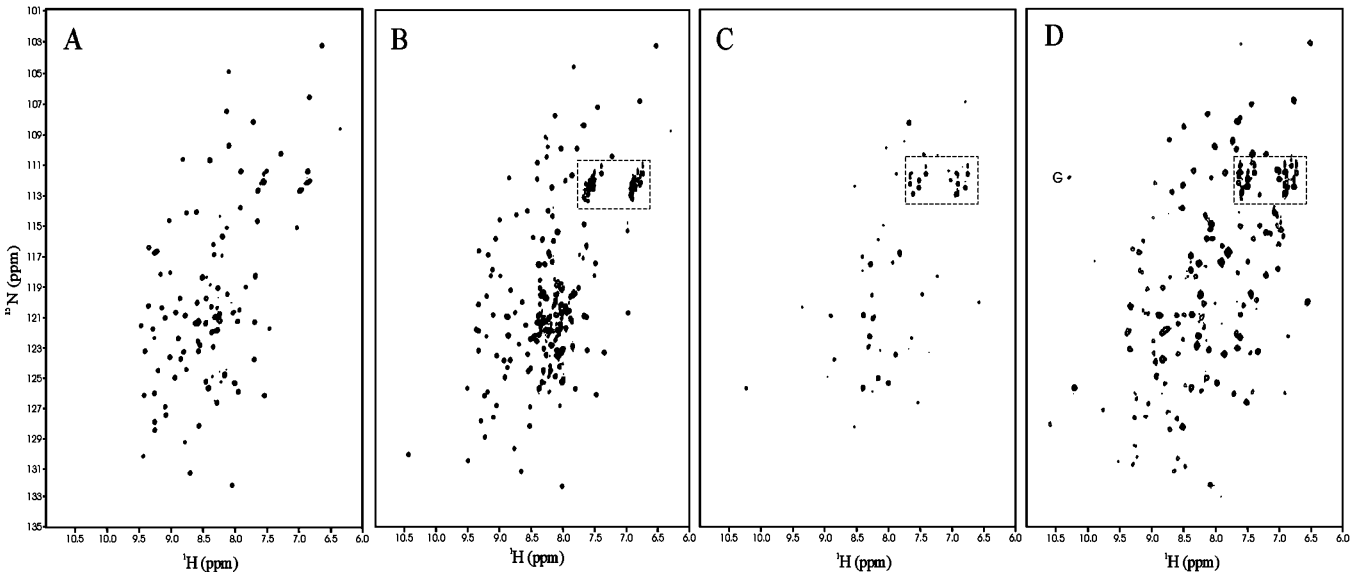

FIGURE 5: Two-dimensional $^{1}H-^{15}N$ HSQC NMR spectra of (A) 0.5 mM uniformly ^{15}N-labeled CipA-X in the presence of 5 mM EDTA, (B) 0.5 mM uniformly ^{15}N-labeled DocX in the presence of 5 mM EDTA, (C) 5 mM $CaCl_2$, and (D) same as (C) at 2.5 times lower vertical scale. All spectra were recorded at pH 7.0, 25 °C, and 11.7 T. The dashed boxes enclose the side-chain H^N resonances, while the solid box encloses a backbone H^N resonance corresponding to G140 from the second EF-hand of the dockerin module.

tor calcium binding to uniformly ^{15}N-labeled DocX. A $^{1}H-^{15}N$ HSQC spectrum of the 172-residue apo-DocX construct, shown in Figure 5B, displayed overall good chemical shift dispersion of $^{1}H-^{15}N$ correlation resonances, with the approximate number of resonances expected, including a large number of well-resolved resonances with H^N chemical shifts > 8.5 ppm. Comparison with the $^{1}H-^{15}N$ HSQC spectrum of the isolated X module, displayed in Figure 5A, suggest that these resonances correspond primarily to backbone H^N groups of the X module, which has a stable tertiary structure in solution (*44*). A clustering of intense resonances with H^N chemical shifts in the random coil region of 8.0−8.5 ppm was also observed. These data are consistent with the CD studies and are indicative of a well-ordered protein comprising significant extended or β-structure and unstructured regions of high flexibility. The narrow line widths further suggested that apo-DocX was in a monomeric state in solution at a concentration of 0.5 mM.

Addition of calcium to saturating concentrations resulted in extensive broadening of most backbone H^N resonances (Figure 5C). A small number of intense resonances between 7.8 and 8.2 ppm remained visible, suggestive that a mobile region in the calcium-bound form exists, as were several side-chain H^N resonances (Figure 5C, dashed box). Only upon adjustment of the vertical scale were many more resonances visible (Figure 5D). Calcium-binding to DocX resulted in an increase in the dispersion of backbone H^N resonances, particularly in the 8.0−8.5 ppm region, and indicated that a region comprising residues primarily from the dockerin module underwent a calcium-induced folding event that stabilized secondary and tertiary structure. Not only do these results corroborate our CD studies but also they are similar to results from the NMR calcium-binding studies of the type I CelS dockerin module of *C. thermocellum* (*28*), where the type I dockerin underwent calcium-induced folding. However, in contrast to our present observations, there was no change in oligomeric state of the type I dockerin upon calcium binding.

Two additional differences between the apo- and Ca-DocX spectra can be correlated to the EF-hand calcium-binding loops of DocX. The appearance of a backbone H^N resonance at 10.3 ppm in the ^{1}H dimension and 112.5 ppm in the ^{15}N dimension is located in a region typical of backbone H^N resonances of the invariant glycine residue at position 6 of the EF-hand calcium-binding loop when in the calcium-bound form. Triple-resonance HNCA data confirmed the identity of this H^N resonance as a backbone H^N of a glycine residue (data not shown), further suggesting that it is the dockerin module of the DocX construct that is undergoing a structural change. Increased dispersion of the side-chain H^N resonances was also observed in the spectra of Ca-DocX (Figure 5C,D). Nine of the total 14 side-chain NH_2-containing residues in DocX reside in the dockerin module, six of which are found in the EF-hand calcium-binding loops (Figure 1D). Structural studies of other EF-hand calcium-binding protein have shown these loops to be quite flexible in the absence of calcium and are consistent with the lack of dispersion of the intense side-chain H^N resonances in the spectrum of apo-DocX (Figure 5A). An increase in the dispersion of NH_2 side-chain resonances of Ca-DocX is consistent with the increased rigidity of the calcium-binding loops due to coordination of the calcium ion. In contrast, there were no observable changes in the $^{1}H-^{15}N$ HSQC NMR spectrum of DocX upon addition of magnesium (data not shown). This observation indicates that the conformational change caused by calcium binding is specific and that the aspartate amino acids located at position 12 of each EF-hand calcium-binding loop in type II dockerin do not alter their specificity for calcium.

Oligomeric State of Ca-DocX. The extensive broadening of NMR resonances in the $^{1}H-^{15}N$ HSQC spectrum of Ca-DocX signified a potential calcium-induced change in the oligomeric state of DocX. Size-exclusion chromatography, multiangle light scattering, and analytical ultracentrifugation were employed to determine the oligomeric state of apo- and Ca-DocX in solution (Table 1). As shown in Figure 6A, the

Table 1: Molecular Masses of DocX in the Absence and Presence of Calcium as Determined by SEC, MALS and AUC

method	Apo-DocX (10^3 Da)	Ca-DocX (10^3 Da)	K_d (μM)
theoretical	18.86	18.86	
SEC[a]	28	33	
MALS[b]	20.43 ± 0.63	43.72 ± 4.30	
AUC[c]	20	31	38

[a] Size-exclusion chromatography. [b] Multiangle light scattering. [c] Analytical ultracentrifugation.

chromatogram of apo-DocX comprised a symmetric peak eluting at 68 mL corresponding to a molecular mass of 28 kDa while Ca-DocX eluted at 64 mL, equivalent to a molecular mass of 33 kDa. The predicted molecular masses of apo- and Ca-DocX are both larger than the theoretical monomeric mass of 18.8 kDa, and the Ca-DocX elution profile had a noticeable tail superseding the main elution peak, suggesting that in the presence of calcium DocX is in an equilibrium of various oligomeric states. However, the elution volume of a protein from size exclusion is dependent on both molecular shape and mass.

To eliminate this shape effect and attain a more accurate molecular mass, as well as gain more comprehensive knowledge of the oligomeric state of DocX in solution, we used a size-exclusion−multiangle light scattering (MALS) tandem system and sedimentation equilibrium analytical ultracentrifugation (AUC). In the MALS experiment, molecular mass was calculated from the refractive index measurement, which is highly dependent on molecular mass and much less dependent on shape (*42*) (Table 1). Apo-DocX had a refractive index corresponding to a molecular mass of 20.43 kDa, or to a monomeric species in solution, while the refractive index for Ca-DocX suggested a dimeric molecular mass of 43.7 kDa. By fitting of the sedimentation equilibrium AUC data to a single-species model, the apparent weight-average molecular masses of the apo- and Ca-DocX were approximately 20 and 31 kDa (Table 1, Figure 6B,C), respectively, which suggests that DocX self-associates in the presence of calcium. This was further corroborated by molecular weight vs concentration analysis, which showed a concentration-dependent association of Ca-DocX (data not shown). Calculation of dissociation constants (K_d) used the monomeric molecular mass of 18 900 Da (Table 1) and a molar extinction coefficient of 15 930 M^{-1} cm^{-1} and estimated the monomer−dimer dissociation constant for Ca-DocX to be approximately 40 μM.

Sedimentation velocity experiments were also performed to examine the hydrodynamic properties of Ca-DocX (data not shown). Sedimentation profiles were evaluated by a continuous distribution $c(S)$ Lamm equation model. When the sedimentation coefficient distribution was determined, a major peak at 2.49 S ($S_{20,w}$ = 2.56 S) with minor peaks at both 1.26 S ($S_{20,w}$ = 1.30 S) and 4.47 S ($S_{20,w}$ = 4.60 S) were revealed. These peaks corresponded to molecular masses of approximately 40.1, 14.4, and 86.0 kDa, respectively, consistent with a predominantly monomer−dimer interaction for Ca-DocX but also showing the formation of higher order oligomers. The velocity data were also exploited to crudely model the shape of the Ca-DocX. A frictional ratio, f/f_0, of 1.65 was calculated for Ca-DocX, implying that Ca-DocX takes on a more elongated or asymmetric shape in solution.

Formation of a 1:1 Type II Dockerin−Cohesin Complex. The calcium-dependent type II dockerin−cohesin interaction, which mediates the attachment of CipA to the cell surface of *C. thermocellum*, is expected to have a stoichiometry of 1:1, on the basis of biochemical, biophysical, and structural studies of the type I interaction (*30*, *32*−*34*, *49*), yet in the present study we observed that DocX homodimerizes in the presence of calcium. To address the biological significance of this dimerization, the type II dockerin−cohesin complex was formed in the presence of excess cohesin and purified by size-exclusion chromatography. As shown in Figure 7, two symmetrical peaks, eluting at 60.4 and 71.9 mL, were observed (labeled 2 and 3) and corresponded to molecular masses of 36 and 21.8 kDa, respectively. Analysis by SDS−PAGE showed two bands of equal intensity for the first elution peak, migrating with molecular masses of 20 and 17 kDa, respectively, while a single band migrating at 20 kDa was observed for the second elution peak (Figure 7 inset). The 20 kDa band in both the elution peaks corresponds well with the molecular mass of cohesin, while the 17 kDa band from the first elution peak migrates at the same molecular mass as that of purified recombinant DocX (lane 4, Figure 7 inset). The molecular mass of the complex, determined from elution volume, and the equal intensity of the two bands in SDS−PAGE, is indicative of a 1:1 Ca-DocX−SdbA type II cohesin complex.

DISCUSSION

To identify the underlying structural elements dictating the specificity of the type I and type II dockerin−cohesin interactions in the cellulosome of *C. thermocellum*, we have generated and characterized a type II dockerin module construct, comprising the C-terminal Doc module and the adjacent hydrophilic X-module from CipA of the *C. thermocellum* cellulosome (DocX). Our observations have been rationalized on the basis of comparisons with CelS type I dockerin module, other typical EF-hand containing proteins, and the type I dockerin−cohesin crystal structure.

The insolubility of the isolated Doc module construct across a range of concentrations (micromolar to millimolar) led to the design of the DocX modular pair construct (Figure 1), which is soluble at millimolar concentrations in both the absence and presence of calcium. We attribute this increased solubility to the high content of acidic/basic residues in the hydrophilic X-module, which has been shown to be highly soluble and folded in native conditions (*44*). The use of chimeric constructs to increase the solubility of proteins of interest has become a common practice and frequently involves the use of thioredoxin, GST, and MBP fusion expression systems. Recombinant fusion proteins have also been previously used in the study of cellulosomal protein modules. A family 2a cellulose-binding domain (CBD) (*50*) was used to enhance the soluble expression of EngB cellulase; the first two studies characterizing the type II dockerin−cohesin interaction used chimeric protein constructs comprising the Doc module fused to the CelC endoglucanase (*21*, *25*); and isothermal titration calorimetry studies carried out to support the recent type I cohesin−dockerin crystal structure used a type I dockerin−Xyn 10B family 22 carbohydrate-binding module chimera. In these latter studies, the authors suggest that the fusion construct provided protection from proteases, including via localization

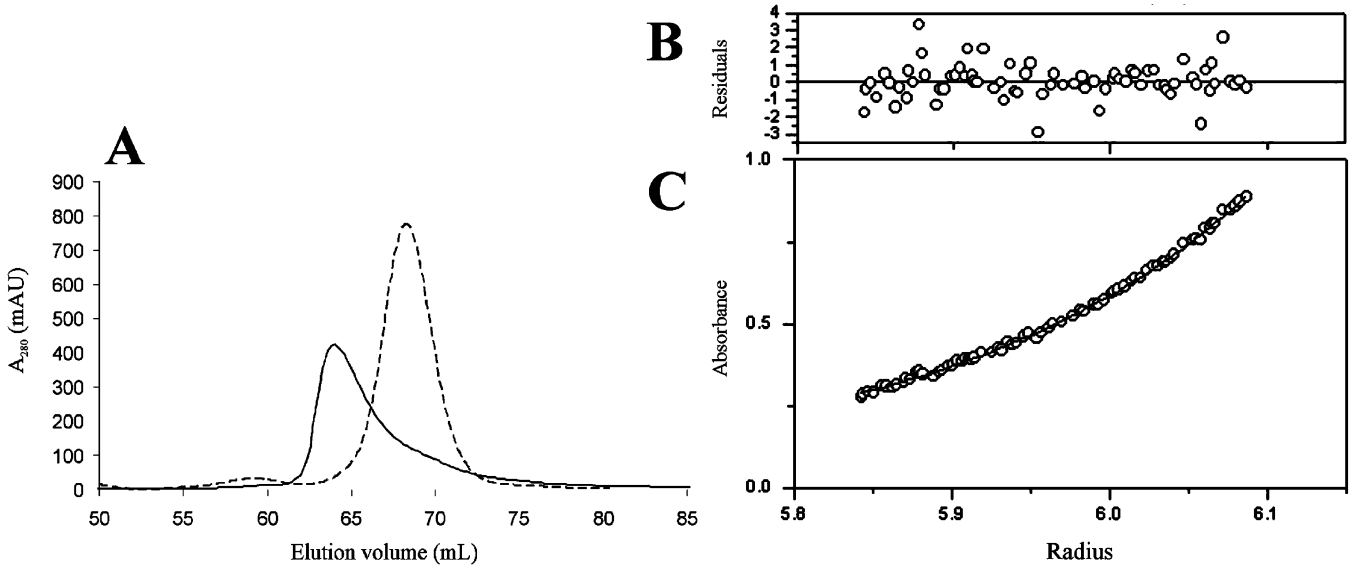

FIGURE 6: Analysis of the oligomeric solution state of Ca-DocX by size-exclusion chromatography and sedimentation equilibrium analysis. (A) Elution profile of purified apo-DocX (---) and Ca-DocX (—) from a Superdex 75 (16/60) size exclusion column. Panels B and C show residual and absorbance plots, respectively, from a sedimentation equilibrium run of Ca-DocX. (○) UV absorbance gradient in the centrifuge cell. The data were fitted to a monomer−dimer equilibrium and the solid line denotes the fitted curve calculated from three rotor speeds and multiple protein concentrations. Residuals show the difference in the fitted and experimental values as a function of radial position.

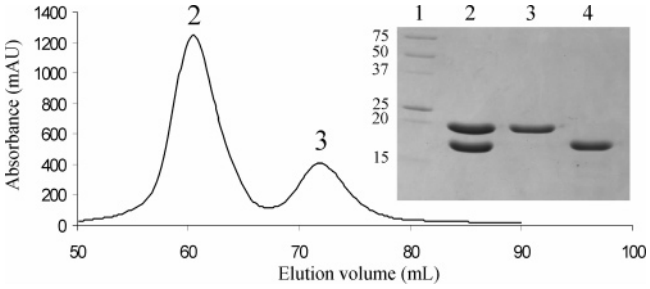

FIGURE 7: Formation of a 1:1 type II dockerin−cohesin complex: size-exclusion chromatographic profile of a 1.5:1 mixture of SdbA type II cohesin and Ca-DocX from a Superdex 75 (16/60) column in the presence of 25 mM HEPES, pH 7.0, 25 mM NaCl, 5 mM DTT, 5 mM $CaCl_2$. (Inset) SDS−PAGE analysis of size-exclusion profile. Lane 1, molecular weight markers; lane 2, sample from elution fraction of peak 2; lane 3, sample from elution fraction of peak 3; lane 4, purified recombinant DocX.

to inclusion bodies, which is where the Doc and DocX constructs in the present study were found. On the basis of the results presented here, the CelC endoglucanase subunit likely also played a significant role in the solubility of the Doc upon refolding. Importantly, DocX represents the in vivo structural architecture of the C-terminal region of CipA.

Using a variety of biophysical techniques, we have shown that the type II dockerin module in the DocX modular pair undergoes a calcium-induced folding event. The CD spectrum and the well-dispersed resonances, including the large number of downfield-shifted resonances (>8.5 ppm), in the $^1H-^{15}N$ HSQC spectrum of apo-DocX (Figure 5A), have similar spectral features to those of isolated CipA X-module (*44*). Because the CD and NMR spectra of isolated CipA X-module are not affected by the addition of calcium (data not shown), the calcium-induced increase in α-helical content and change in tertiary structure can be attributed to calcium binding to the type II dockerin module. This suggestion is further substantiated by comparisons with structural studies of the type I dockerin module. The calcium-mediated increase in NMR spectral dispersion we observed for DocX is similar to that observed in the NMR structural studies of CelS type I dockerin (*28*) and indicate that calcium is required to maintain a globular fold for both CelS type I dockerin and CipA type II dockerin. Furthermore, the 7 μM calcium dissociation constant we have determined for type II dockerin corresponds well with the slow exchange observed in NMR calcium binding studies of type I dockerin (*28*). A single downfield-shifted resonance in the spectrum of Ca-DocX, corresponding to a glycine, has a backbone amide chemical shift (10.3 ppm) very similar to those observed for glycine residues at position 6 of EF-hand calcium-binding loops in Ca-TnC (10.3−10.8 ppm) (*51*), Ca-CaM (10.3−10.7 ppm) (*52*), S100B (10.1 ppm) (*53*, *54*), and CelS type I dockerin (10.0−10.2 ppm) (*28*). These glycine residues form a central hinge in the calcium-binding loop, resulting in a unique downfield-shifted position of their backbone H^N resonance. However, we cannot rule out the possibility that the calcium-induced conformational changes in the dockerin module may propagate into the X module.

MALS and AUC experiments show that DocX undergoes calcium-induced homodimerization. The notion is supported by the observation that calcium binding to DocX caused significant line broadening of several resonances in the NMR spectrum, suggesting a change in thestate of oligomerization. Other EF-hand proteins, including troponin C and S100B (*53*, *55*) display similar behavior, which has been associated with a calcium-dependent conformational change that exposes a hydrophobic region necessary for interactions with hydrophobic elements of a target protein. Our ANS results support the increased exposure of a hydrophobic region in the type II dockerin module upon calcium binding and leads to the possibility that homodimerization may be mediated, at least in part, by hydrophobic interactions. Interestingly, the presence of SdbA type II cohesin results in the dissociation of the DocX dimer and the formation of a 1:1 Ca-DocX−SdbA type II cohesin complex. The ability of SdbA type II cohesin to break up the Ca-DocX dimer through a noncovalent interaction with Ca-DocX suggests that the

area involved in the homodimeric interface may be part of, or at least in close proximity to, the type II cohesin-binding site. Parallel behavior is observed for type I cohesin modules: type I cohesin modules of *C. thermocellum* and the cohesin modules of *C. cellulolyticum* self-associate, and this association is disrupted upon formation of the cohesin−dockerin complex. Structural analysis and mutation studies confirmed the overlap between the regions involved in homodimer formation and binding of the dockerin module (*30*, *56*−*60*). The elongated shape of Ca-DocX, suggested by sedimentation velocity data, may arise from the formation of a dockerin−X-module interface in the presence of calcium, or the dimerization event, or from a combination of the previous two situations. Detailed structural analysis will be required to definitively identify the origin of the elongated shape.

The homodimerization of Ca-DocX is in direct contrast to calcium-bound CelS type I dockerin, which remained monomeric in solution (*29*). However, despite strong sequence similarities, there are five significant substitutions in DocX that would increase the hydrophobic nature of the exposed surface (Figure 1C): Leu, rather than Ser and Thr, is at positions 17 and 18 in DocX; an Ile resides at position 24 that is a Lys in the type I dockerin sequence; and the Ser and Thr at positions 49 and 50 are Met and Gln at the corresponding positions in DocX. Furthermore, the coinciding loss of hydrogen-bonding (Ser/ Thr -OH) and electrostatic character (Lys NH_3^+) would decrease the ability of the dockerin module to favorably interact with the solvent and remain monomeric in solution, as seen for CelS type I dockerin (*29*). Thus, some or all of these residues may contribute to the enhanced tendency of DocX to form dimers. They could also include residues involved in the formation of the cohesin−dockerin complex and in determining the specificity of the interaction. Determination of a type II dockerin−cohesin complex is currently underway to identify the structural differences driving the specificity of the type I and type II interactions.

ACKNOWLEDGMENT

We thank Pierre Béguin for supplying the pCip102 clone and for helpful discussions as well as Kim Munro for assistance with CD data collection and interpretation.

REFERENCES

1. Lamed, R., Kenig, R., Setter, E., and Bayer, E. A. (1983b) The cellulosome: a discrete cell surface organelle of *Clostridium thermocellum* which exhibits separate antigenic, cellulolose-binding and various cellulolytic activities, *Biotechnol. Bioeng. Symp. 13*, 163−181.
2. Lamed, R., Setter, E., and Bayer, E. A. (1983a) Characterization of a cellulose-binding, cellulase-containing complex in *Clostridium thermocellum*, *J. Bacteriol. 156*, 828−36.
3. Pages, S., Belaich, A., Tardif, C., Reverbel-Leroy, C., Gaudin, C., and Belaich, J. P. (1996) Interaction between the endoglucanase CelA and the scaffolding protein CipC of the *Clostridium* cellulolyticum cellulosome, *J. Bacteriol. 178*, 2279−86.
4. Gal, L., Pages, S., Gaudin, C., Belaich, A., Reverbel-Leroy, C., Tardif, C., and Belaich, J. P. (1997) Characterization of the cellulolytic complex (cellulosome) produced by *Clostridium cellulolyticum*, *Appl. Environ. Microbiol. 63*, 903−9.
5. Doi, R. H., Goldstein, M., Hashida, S., Park, J. S., and Takagi, M. (1994) The *Clostridium cellulovorans* cellulosome, *Crit. Rev. Microbiol. 20*, 87−93.
6. Kakiuchi, M., Isui, A., Suzuki, K., Fujino, T., Fujino, E., Kimura, T., Karita, S., Sakka, K., and Ohmiya, K. (1998) Cloning and DNA sequencing of the genes encoding *Clostridium josui* scaffolding protein CipA and cellulase CelD and identification of their gene products as major components of the cellulosome, *J. Bacteriol. 180*, 4303−8.
7. Ding, S. Y., Bayer, E. A., Steiner, D., Shoham, Y., and Lamed, R. (1999) A novel cellulosomal scaffoldin from *Acetivibrio cellulolyticus* that contains a family 9 glycosyl hydrolase, *J. Bacteriol. 181*, 6720−9.
8. Xu, Q., Gao, W., Ding, S. Y., Kenig, R., Shoham, Y., Bayer, E. A., and Lamed, R. (2003) The cellulosome system of *Acetivibrio cellulolyticus* includes a novel type of adaptor protein and a cell surface anchoring protein, *J. Bacteriol. 185*, 4548−57.
9. Ding, S. Y., Bayer, E. A., Steiner, D., Shoham, Y., and Lamed, R. (2000) A scaffoldin of the *Bacteroides cellulosolvens* cellulosome that contains 11 type II cohesins, *J. Bacteriol. 182*, 4915−25.
10. Xu, Q., Bayer, E. A., Goldman, M., Kenig, R., Shoham, Y., and Lamed, R. (2004) Architecture of the *Bacteroides cellulosolvens* cellulosome: description of a cell surface-anchoring scaffoldin and a family 48 cellulase, *J. Bacteriol. 186*, 968−77.
11. Ding, S. Y., Rincon, M. T., Lamed, R., Martin, J. C., McCrae, S. I., Aurilia, V., Shoham, Y., Bayer, E. A., and Flint, H. J. (2001) Cellulosomal scaffoldin-like proteins from *Ruminococcus flavefaciens*, *J. Bacteriol. 183*, 1945−53.
12. Steenbakkers, P. J., Li, X. L., Ximenes, E. A., Arts, J. G., Chen, H., Ljungdahl, L. G., and Op Den Camp, H. J. (2001) Noncatalytic docking domains of cellulosomes of anaerobic fungi, *J. Bacteriol. 183*, 5325−33.
13. Bhat, K. M., and Wood, T. M. (1992) The cellulase of anaerobic bacterium *Clostridium thermocellum*—isolation, dissociation, and resassociation of the cellulosome, *Carbohydr. Res. 227*, 293−300.
14. Bhat, S., Goodenough, P. W., Bhat, M. K., and Owen, E. (1994) Isolation of four major subunits from *Clostridium thermocellum* cellulosome and their synergism in the hydrolysis of crystalline cellulose, *Int. J. Biol. Macromol. 16*, 335−42.
15. Bayer, E. A., Morag, E., and Lamed, R. (1994) The cellulosome—a treasure-trove for biotechnology, *Trends Biotechnol. 12*, 379−86.
16. Tokatlidis, K., Salamitou, S., Beguin, P., Dhurjati, P., and Aubert, J. P. (1991) Interaction of the duplicated segment carried by *Clostridium thermocellum* cellulases with cellulosome components, *FEBS Lett. 291*, 185−8.
17. Tokatlidis, K., Dhurjati, P., and Beguin, P. (1993) Properties conferred on *Clostridium thermocellum* endoglucanase CelC by grafting the duplicated segment of endoglucanase CelD, *Protein Eng. 6*, 947−52.
18. Fujino, T., Beguin, P., and Aubert, J. P. (1993) Organization of a *Clostridium thermocellum* gene cluster encoding the cellulosomal scaffolding protein CipA and a protein possibly involved in attachment of the cellulosome to the cell surface, *J. Bacteriol. 175*, 1891−9.
19. Gerngross, U. T., Romaniec, M. P., Kobayashi, T., Huskisson, N. S., and Demain, A. L. (1993) Sequencing of a *Clostridium thermocellum* gene (cipA) encoding the cellulosomal SL-protein reveals an unusual degree of internal homology, *Mol. Microbiol. 8*, 325−34.
20. Fujino, T., Beguin, P., and Aubert, J. P. (1992) Cloning of a *Clostridium thermocellum* DNA fragment encoding polypeptides that bind the catalytic components of the cellulosome, *FEMS Microbiol. Lett. 73*, 165−70.
21. Salamitou, S., Raynaud, O., Lemaire, M., Coughlan, M., Beguin, P., and Aubert, J. P. (1994) Recognition specificity of the duplicated segments present in *Clostridium thermocellum* endoglucanase CelD and in the cellulosome-integrating protein CipA, *J. Bacteriol. 176*, 2822−7.
22. Yaron, S., Morag, E., Bayer, E. A., Lamed, R., and Shoham, Y. (1995) Expression, purification and subunit-binding properties of cohesins 2 and 3 of the *Clostridium thermocellum* cellulosome, *FEBS Lett. 360*, 121−4.
23. Lytle, B., Myers, C., Kruus, K., and Wu, J. H. (1996) Interactions of the CelS binding ligand with various receptor domains of the *Clostridium thermocellum* cellulosomal scaffolding protein, CipA, *J. Bacteriol. 178*, 1200−3.
24. Jindou, S., Soda, A., Karita, S., Kajino, T., Beguin, P., Wu, J. H., Inagaki, M., Kimura, T., Sakka, K., and Ohmiya, K. (2004) Cohesin−dockerin interactions within and between *Clostridium*

josui and *Clostridium thermocellum*: binding selectivity between cognate dockerin and cohesin domains and species specificity, *J. Biol. Chem. 279*, 9867−74.
25. Leibovitz, E., and Beguin, P. (1996) A new type of cohesin domain that specifically binds the dockerin domain of the *Clostridium thermocellum* cellulosome-integrating protein CipA, *J. Bacteriol. 178*, 3077−84.
26. Leibovitz, E., Ohayon, H., Gounon, P., and Beguin, P. (1997) Characterization and subcellular localization of the *Clostridium thermocellum* scaffoldin dockerin binding protein SdbA, *J. Bacteriol. 179*, 2519−23.
27. Pages, S., Belaich, A., Belaich, J. P., Morag, E., Lamed, R., Shoham, Y., and Bayer, E. A. (1997) Species-specificity of the cohesin-dockerin interaction between *Clostridium thermocellum* and *Clostridium cellulolyticum*: prediction of specificity determinants of the dockerin domain, *Proteins: Struct., Funct., Genet. 29*, 517−27.
28. Lytle, B. L., Volkman, B. F., Westler, W. M., and Wu, J. H. (2000) Secondary structure and calcium-induced folding of the *Clostridium thermocellum* dockerin domain determined by NMR spectroscopy, *Arch. Biochem. Biophys. 379*, 237−44.
29. Lytle, B. L., Volkman, B. F., Westler, W. M., Heckman, M. P., and Wu, J. H. (2001) Solution structure of a type I dockerin domain, a novel prokaryotic, extracellular calcium-binding domain, *J. Mol. Biol. 307*, 745−53.
30. Carvalho, A. L., Dias, F. M., Prates, J. A., Nagy, T., Gilbert, H. J., Davies, G. J., Ferreira, L. M., Romao, M. J., and Fontes, C. M. (2003) Cellulosome assembly revealed by the crystal structure of the cohesin−dockerin complex, *Proc. Natl. Acad. Sci. U.S.A. 100*, 13809−14.
31. Lytle, B., and Wu, J. H. (1998) Involvement of both dockerin subdomains in assembly of the *Clostridium thermocellum* cellulosome, *J. Bacteriol. 180*, 6581−5.
32. Mechaly, A., Yaron, S., Lamed, R., Fierobe, H. P., Belaich, A., Belaich, J. P., Shoham, Y., and Bayer, E. A. (2000) Cohesin−dockerin recognition in cellulosome assembly: experiment versus hypothesis, *Proteins: Struct., Funct., Genet. 39*, 170−7.
33. Mechaly, A., Fierobe, H. P., Belaich, A., Belaich, J. P., Lamed, R., Shoham, Y., and Bayer, E. A. (2001) Cohesin−dockerin interaction in cellulosome assembly: a single hydroxyl group of a dockerin domain distinguishes between nonrecognition and high affinity recognition, *J. Biol. Chem. 276*, 9883−8.
34. Schaeffer, F., Matuschek, M., Guglielmi, G., Miras, I., Alzari, P. M., and Beguin, P. (2002) Duplicated dockerin subdomains of *Clostridium thermocellum* endoglucanase CelD bind to a cohesin domain of the scaffolding protein CipA with distinct thermodynamic parameters and a negative cooperativity, *Biochemistry 41*, 2106−14.
35. Jindou, S., Kajino, T., Inagaki, M., Karita, S., Beguin, P., Kimura, T., Sakka, K., and Ohmiya, K. (2004) Interaction between a type-II dockerin domain and a type-II cohesin domain from *Clostridium thermocellum* cellulosome, *Biosci. Biotechnol. Biochem. 68*, 924−6.
36. Garcia-Campayo, V., and Beguin, P. (1997) Synergism between the cellulosome-integrating protein CipA and endoglucanase CelD of *Clostridium thermocellum*, *J. Biotechnol. 57*, 39−47.
37. Smith, S. P., Beguin, P., Alzari, P. M., and Gehring, K. (2002) ^{1}H, ^{13}C, ^{15}N NMR sequence-specific resonance assignment of a *Clostridium thermocellum* type II cohesin module, *J. Biomol. NMR 23*, 73−4.
38. Bohm, G., Muhr, R., and Jaenicke, R. (1992) Quantitative analysis of protein far UV circular dichroism spectra by neural networks, *Protein Eng. 5*, 191−195.
39. Kay, L. E., Keiffer, P., and Saarinen, T. (1992) Pure absorption gradient enhanced heteronuclear single quantum correlation spectroscopy with improved sensitivity, *J. Am. Chem. Soc. 114*, 10663−10665.
40. Delaglio, F., Grzesiek, S., Vuister, G. W., Zhu, G., Pfeifer, J., and Bax, A. (1995) NMRPipe: a multidimensional spectral processing system based on UNIX pipes, *J. Biomol. NMR 6*, 277−93.
41. Johnson, B. A., and Blevins, R. A. (1994) NMRVIEW: a computer program for the visualization and analysis of NMR data, *J. Biomol. NMR 4*, 603−614.
42. Wyatt, P. J. (1993) Light scattering and the absolute characterization of macromolecules, *Anal. Chim. Acta 272*, 1−40.
43. Schuck, P., Perugini, M. A., Gonzales, N. R., Howlett, G. J., and Schubert, D. (2002) Size-distribution analysis of proteins by analytical ultracentrifugation: strategies and application to model systems, *Biophys. J. 82*, 1096−111.
44. Adams, J. J., Jang, C. J., Spencer, H. L., Elliott, M., and Smith, S. P. (2004) Expression, purification and structural characterization of the scaffoldin hydrophilic X-module from the cellulosome of *Clostridium thermocellum*, *Protein Expression Purif. 38*, 258−263.
45. Zhang, M., Tanaka, T., and Ikura, M. (1995) Calcium-induced conformational transition revealed by the solution structure of apo calmodulin, *Nat. Struct. Biol. 2*, 758−67.
46. Gagne, S. M., Tsuda, S., Li, M. X., Smillie, L. B., and Sykes, B. D. (1995) Structures of the troponin C regulatory domains in the apo and calcium-saturated states, *Nat. Struct. Biol. 2*, 784−9.
47. Smith, S. P., and Shaw, G. S. (1998) A novel calcium-sensitive switch revealed by the structure of human S100B in the calcium-bound form, *Structure 6*, 211−22.
48. Smith, S. P., and Shaw, G. S. (1998) A change-in-hand mechanism for S100 signaling, *Biochem. Cell Biol. 76*, 324−33.
49. Fierobe, H. P., Pages, S., Belaich, A., Champ, S., Lexa, D., and Belaich, J. P. (1999) Cellulosome from *Clostridium cellulolyticum*: molecular study of the Dockerin/Cohesin interaction, *Biochemistry 38*, 12822−32.
50. Murashima, K., Kosugi, A., and Doi, R. H. (2003) Solubilization of cellulosomal cellulases by fusion with cellulose-binding domain of noncellulosomal cellulase engineered from *Clostridium cellulovorans*, *Proteins: Struct., Funct., Genet. 50*, 620−8.
51. Slupsky, C. M., Reinach, F. C., Smillie, L. B., and Sykes, B. D. (1995) Solution secondary structure of calcium-saturated troponin C monomer determined by multidimensional heteronuclear NMR spectroscopy, *Protein Sci. 4*, 1279−90.
52. Ikura, M., Kay, L. E., and Bax, A. (1990) A novel approach for sequential assignment of ^{1}H, ^{13}C, and ^{15}N spectra of proteins: heteronuclear triple-resonance three-dimensional NMR spectroscopy. Application to calmodulin, *Biochemistry 29*, 4659−67.
53. Smith, S. P., Barber, K. R., Dunn, S. D., and Shaw, G. S. (1996) Structural influence of cation binding to recombinant human brain S100b: evidence for calcium-induced exposure of a hydrophobic surface, *Biochemistry 35*, 8805−14.
54. Smith, S. P., and Shaw, G. S. (1997) Assignment and secondary structure of calcium-bound human S100B, *J. Biomol. NMR 10*, 77−88.
55. Slupsky, C. M., Kay, C. M., Reinach, F. C., Smillie, L. B., and Sykes, B. D. (1995) Calcium-induced dimerization of troponin C: mode of interaction and use of trifluoroethanol as a denaturant of quaternary structure, *Biochemistry 34*, 7365−75.
56. Shimon, L. J., Bayer, E. A., Morag, E., Lamed, R., Yaron, S., Shoham, Y., and Frolow, F. (1997) A cohesin domain from *Clostridium thermocellum*: the crystal structure provides new insights into cellulosome assembly, *Structure 5*, 381−90.
57. Tavares, G. A., Beguin, P., and Alzari, P. M. (1997) The crystal structure of a type I cohesin domain at 1.7 A resolution, *J. Mol. Biol. 273*, 701−13.
58. Spinelli, S., Fierobe, H. P., Belaich, A., Belaich, J. P., Henrissat, B., and Cambillau, C. (2000) Crystal structure of a cohesin module from *Clostridium cellulolyticum*: implications for dockerin recognition, *J. Mol. Biol. 304*, 189−200.
59. Miras, I., Schaeffer, F., Beguin, P., and Alzari, P. M. (2002) Mapping by site-directed mutagenesis of the region responsible for cohesin−dockerin interaction on the surface of the seventh cohesin domain of *Clostridium thermocellum* CipA, *Biochemistry 41*, 2115−9.
60. Nakar, D., Handelsman, T., Shoham, Y., Fierobe, H. P., Belaich, J. P., Morag, E., Lamed, R., and Bayer, E. A. (2004) Pinpoint mapping of recognition residues on the cohesin surface by progressive homologue swapping, *J. Biol. Chem. 279*, 42881−8.

BI048039U